Performance and Energy Consumption Analysis of UV-H_2O_2 Photoreactors Using Computational Fluid Dynamics

M. Moghaddami and M. Raisee

***Abstract*—Advanced Oxidation Processes (AOPs) promoted by ultraviolet light are innovative and potentially cost-effective solutions for treating persistent pollutants recalcitrant to conventional water and wastewater treatments. While several studies have been performed during the past decade to improve the fundamental understanding of the UV-H_2O_2 AOP and its kinetic modeling, Computational Fluid Dynamics (CFD) has only recently emerged as powerful tool that allow a deeper understanding of complex photochemical processes in environmental and reactor engineering applications. In this investigation, a comprehensive kinetic model of UV-H_2O_2 AOP was coupled with the Reynolds Averaged Navier-Stokes (RANS) equations and UV fluence rate model using CFD to predict the oxidation of tributyl phosphate (TBP) and tri (2-chloroethtyl) phosphate (TCEP) in two different photoreactors: namely a parallel- and a cross-flow UV device employing a UV lamp emitting primarily the 253.7 nm radiation. The calculation of the fluence rate field was carried out by solving the irradiative transport equation (RTE) using the discrete ordinate(DO) model. Notably, the fluence rate model assumes a fluid with a spatially dependent absorption coefficient that is function of the H_2O_2 and HO_2^- species concentration. The oxidation performance of both reactors is computed and the Electrical Energy per Order (EEO) is computed for the comparison of the reactors and it is found that the EEO of the cross flow reactor is greater.**

***Index Terms*—Hydrogen peroxide; ultra violet; energy consumption; performance.**

I. Introduction

While reclamation and reuse of municipal wastewater is becoming an accepted practice especially in arid and semi-arid regions, emerging micropollutants such as endocrine disruptors and pharmaceutically active compounds are increasingly being detected in limited water sources such as surface water and groundwater. These micropollutants, which are continuously released into the environment after little or no treatment, could be oxidized by Advanced Oxidation Processes (AOPs) such as UV-H_2O_2.

Stefan et al. [1] conducted a study on the kinetics and reaction mechanism of acetone degradation by UV-H_2O_2 in dilute aqueous solution. The investigators proposed a kinetic model that successfully predicted reactant and intermediate profiles. Later, Crittenden et al. [2] advanced a UV-H_2O_2 dynamic kinetic model for a completely mixed batch reactor to predict pollutant removal demonstrating good agreement between observed and predicted data.

Watts and Linden [3] reported on the UV-H_2O_2 oxidation of tri-n-butyl phosphate (TBP) and tri (2-chloroethyl) phosphate (TCEP) using a monochromatic (253.7 nm) collimated beam UV reactor. They observed that direct photolysis of both contaminants was not a relevant process. They also concluded that TCEP needed an order of magnitude higher UV dose to achieve the same level of removal as TBP.

Lately, the prediction of the fluence rate distribution in a UV-H_2O_2 reactor has also received considerable attention. Bolton [4] presented a model which accounted for both reflection and refraction as the UV beam goes through the air/quartz/water interfaces. Liu et al. [5] investigated the performance of various radiation models and concluded that the effects of refraction must be taken into consideration for accurate simulation of fluence rate distribution, as confirmed in a subsequent paper by Sasges et al. [6] who proposed the use of a Lambertian type model (i.e., MSSS).

The reactor hydraulics has also been studied in depth by several investigators. Sozzi and Taghipur [7] investigated turbulent flows through complex L-shape and U-shape UV-reactors and examined the influence of three different turbulence models (Standard k-ε, Realizable k-ε, and Reynolds stress model) on the predicted results. Results indicated that Realizable k-ε produced the best overall prediction of the experimental PIV measurements.

Shao [8] and Hofman et al. [9] performed numerical computations for a 4-lamp closed vessel UV reactor using three different cross-flow configurations (staggered, squared and trapezoidal) to investigate the role of reactor hydraulics on UV dose distribution. Among the three cases examined, the staggered lamp arrangement (e.g., UV lamps positioned with a relative vertical offset in the flow direction) predicted a UV dose distribution with the highest mean UV dose and the lowest variance.

Recently, Alpert [10] investigated the use of CFD to evaluate the performance of a comprehensive UV/AOP degradation of an indicator organic contaminant (methylene blue). They found that the CFD model under-predicted the experimental percent removal of methylene blue and that its degradation was sensitive to the background dissolved organic carbon concentration.

In this paper, the steady state hydroxyl radical distribution in two hypothetical UV-H_2O_2 photoreactors was investigated using a CFD approach. The yield of removal and EEO efficiency (electrical energy per unit flow per log removal) were predicted for both TCEP and TBP oxidation (pollutants that are increasingly detected in municipal water and

Manuscript received May 26, 2012; revised July 8, 2012.

Authors are with the School of Mechanical Engineering, College of Engineering, University of Tehran, Tehran, Iran. (e-mail: moghaddamy@yahoo.com; mraisee@ut.ac.ir)

wastewater [11] and artificially recharged groundwater [12]. Given the considerable contribution of hydrogen peroxide (50 mg/L) to fluid absorption coefficient, the species transport, chemical reactions, and UV fluence rate sub-models have been fully coupled in our model using a spatially dependent fluid absorption coefficient (function of the local hydroxyl peroxide concentration). The CFD model is used to evaluate and compare the energy consumption of annular and cross flow reactors.

II. Methods

A. Governing Equations

All the flow and mass transfer equations are presented in Cartesian tensor notation. For a steady incompressible flow, the conservation laws of mass, momentum and concentration are written as:

Continuity:

$$\frac{\partial U_j}{\partial x_j} = 0 \tag{1}$$

Momentum:

$$\frac{\partial (U_j U_i)}{\partial x_j} = \frac{-1}{\rho}\frac{\partial P}{\partial x_i} + \frac{\partial}{\partial x_j}\left(\nu \frac{\partial U_i}{\partial x_j} - \overline{u_i u_j}\right) \tag{2}$$

Mass species:

$$\frac{\partial (U_j Y_i)}{\partial x_j} = \frac{\partial}{\partial x_j}\left(\frac{\nu}{Sc}\frac{\partial Y_i}{\partial x_j} - \overline{u_j y_i}\right) + R_i \tag{3}$$

where ρ, ν and Sc are respectively, the density, the kinematic viscosity and the Schmidt number.

In equation (3) R_i represents the net rate of production by chemical reaction for each component included in the CFD model.

B. Turbulence Model

In this study, the standard high-Re k-ε model was used to describe turbulent flows in annular reactor. Such choice is justified by the extreme simplicity of the flow field in an annular reactor, where the standard high-Re k-ε model is expected to provide reasonable results. The standard k-ε model is a semi-empirical model based on model transport equations for the turbulence kinetic energy (k) and its dissipation rate (ε). In this turbulence model, Reynolds stresses ($-\rho\overline{u_i u_j}$) and mass transfer diffusion ($-\rho\overline{u_i y_j}$) terms are obtained from the eddy-viscosity and eddy-diffusivity approximations given in equations (4) and (5) respectively:

$$\overline{u_i u_j} = 2/3\,\delta_{ij}k - \nu_t\left(\frac{\partial U_i}{\partial x_j} + \frac{\partial U_j}{\partial x_i}\right) \tag{4}$$

$$\overline{u_i y_j} = -\frac{\nu_t}{Sc_T}\frac{\partial Y_j}{\partial x_i} \tag{5}$$

where the turbulent viscosity, ν_t, is obtained from:

$$\nu_t = C_\mu \frac{k^2}{\varepsilon} \tag{6}$$

and the value of constants C_μ , and turbulent Schmidt number (Sc_T) are given in Table I.

The turbulence kinetic energy, k, and its rate of dissipation, ε, are obtained from the following transport equations:

$$\frac{\partial}{\partial x_j}\left(U_j k\right) = \frac{\partial}{\partial x_j}\left[\left(\nu + \frac{\nu_t}{\sigma_k}\right)\frac{\partial k}{\partial x_j}\right] + P_k - \varepsilon \tag{7}$$

$$\frac{\partial}{\partial x_j}\left(U_j \varepsilon\right) = \frac{\partial}{\partial x_j}\left[\left(\nu + \frac{\nu_t}{\sigma_\varepsilon}\right)\frac{\partial \varepsilon}{\partial x_j}\right] + C_{\varepsilon 1}\frac{\varepsilon}{k}P_k - C_{\varepsilon 2}\frac{\varepsilon^2}{k} \tag{8}$$

In the above equations P_k is the generation rate of turbulent kinetic energy obtained from:

$$P_k = -\overline{u_i u_j}\frac{\partial U_i}{\partial x_j} \tag{9}$$

All constants appearing in the above equations are given in Table I.

TABLE I: EMPIRICAL CONSTANTS OF THE K-E TURBULENCE MODEL

ScT	σε	σk	Cε2	Cε1	Cμ
0.7	1.3	1.0	1.92	1.44	0.09

C. The Kinetic Model for UV-H2O2 Advanced Oxidation

Table II summarizes the photochemical and chemical reactions incorporated in the CFD model, along with their rate constants.

The detailed UV-H_2O_2 kinetic model has been extensively validated in several previous studies and particularly in Crittenden et al. [2] for continuous flow stirred tank reactors and Li et al. [13], who implemented the UV-H_2O_2 reaction mechanism in the AdOx software. The kinetic model was incorporated into CFD using numerical subroutines to prescribe the net rate of generation for each chemical species considered.

D. Fluence Rate Model

The calculation of the fluence rate field was carried out by solving the radiation transport equation (RTE) using the discrete ordinate model [14]. In the discrete ordinate (DO) model, the RTE is solved for the spectral intensity $I_\lambda(\vec{r},\vec{s})$:

$$\nabla.\left(I_\lambda(\vec{r},\vec{s}),\vec{s}\right) + a_\lambda I_\lambda(\vec{r},\vec{s}) = 0 \tag{10}$$

where $\vec{r}$ and $\vec{s}$ are position and direction vectors respectively, λ is the wavelength and a_λ is the spectral, spatially-dependent fluid absorption coefficient.

In order to account for refraction, the air gap separating the lamp and the quartz sleeve regions has been included in the computational domain. Refractive indexes for air and water were assumed to be 1 and 1.37, respectively.

TABLE II: THE KINETIC MODEL OF UV-H2O2 ADVANCED OXIDATION OF PHOSPHATE ESTERS ([13]).

No.	Reactions	Rate Constants, $M^{-1}s^{-1}$	Reference
1	$H_2O_2 / HO_2^- + h\upsilon \rightarrow 2OH\bullet$	$r_{UV,H_2O_2}^{local} = -2.303\phi_{H_2O_2} I (\varepsilon_{H_2O_2}[H_2O_2] + \varepsilon_{HO_2^-}[HO_2^-])$	[15]
2	$H_2O_2 + OH\bullet \rightarrow H_2O + HO_2\bullet$	$k_2 = 2.7\times10^7$	[16]
3	$OH\bullet + HO_2^- \rightarrow HO_2\bullet + OH^-$	$k_3 = 7.5\times10^9$	[17]
4	$H_2O_2 + HO_2\bullet \rightarrow OH\bullet + H_2O + O_2$	$k_4 = 3$	[18]
5	$H_2O_2 + O_2^-\bullet \rightarrow OH\bullet + O_2 + OH^-$	$k_5 = 0.13$	[19]
6	$OH\bullet + CO_3^{2-} \rightarrow CO_3^-\bullet + OH^-$	$k_6 = 3.9\times10^8$	[16]
7	$OH\bullet + HCO_3^- \rightarrow CO_3^-\bullet + H_2O$	$k_7 = 8.5\times10^6$	[16]
8	$H_2O_2 + CO_3^-\bullet \rightarrow HCO_3^- + HO_2\bullet$	$k_8 = 4.3\times10^5$	[20]
9	$HO_2^- + CO_3^-\bullet \rightarrow CO_3^{2-} + HO_2\bullet$	$k_9 = 3.0\times10^7$	[20]
10	$OH\bullet + OH\bullet \rightarrow H_2O_2$	$k_{10} = 5.5\times10^9$	[16]
11	$OH\bullet + HO_2\bullet \rightarrow H_2O + O_2$	$k_{11} = 6.6\times10^9$	[21]
12	$HO_2\bullet + HO_2\bullet \rightarrow H_2O_2 + O_2$	$k_{12} = 8.3\times10^5$	[22]
13	$HO_2\bullet + O_2^-\bullet \rightarrow HO_2^- + O_2$	$k_{13} = 9.7\times10^7$	[22]
14	$OH\bullet + O_2^-\bullet \rightarrow O_2 + OH^-$	$k_{14} = 7.0\times10^9$	[23]
15	$OH\bullet + CO_3^-\bullet \rightarrow ?$	$k_{15} = 3.0\times10^9$	[24]
16	$CO_3^-\bullet + O_2^-\bullet \rightarrow CO_3^{2-} + O_2$	$k_{16} = 6.0\times10^8$	[25]
17	$CO_3^-\bullet + CO_3^-\bullet \rightarrow ?$	$k_{17} = 3.0\times10^7$	[26]
18	$OH\bullet + TCEP \rightarrow TCEP_{products}$	$k_{18} = k_{TCEP} = 5.6\times10^8$	[27]
19	$OH\bullet + TBP \rightarrow TBP_{products}$	$k_{19} = k_{TBP} = 6.4\times10^9$	[27]
20	$H_2CO_3 \Leftrightarrow H^+ + HCO_3^-$	$pK_{a1} = 6.3$	[28]
21	$HCO_3^- \Leftrightarrow H^+ + CO_3^{2-}$	$pK_{a2} = 10.3$	[28]
22	$H_2O_2 \Leftrightarrow H^+ + HO_2^-$	$pK_{a3} = 11.6$	[29]
23	$HO_2\bullet \Leftrightarrow H^+ + O_2^-\bullet$	$pK_{a4} = 4.8$	[29]

E. UV-H_2O_2 Photoreactors

The oxidation of phosphate esters by UV-H_2O_2 was investigated in two different photoreactors, namely a single-lamp axi-symmetric annular and a single-lamp cross-flow UV system. Their schematic representations are shown in Fig. 1, respectively, with dimensions given in centimeters.

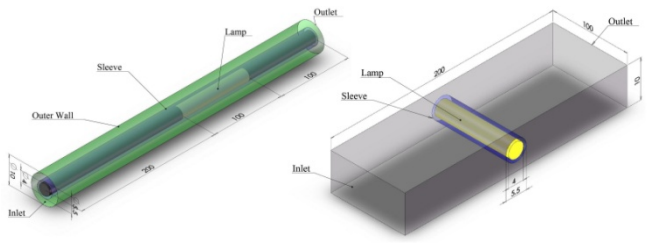

Fig. 1. Schematic representation of the annular UV (left) and cross-flow (right) photoreactors (dimensions are given in centimeters)

Each reactor consists of a 4-cm diameter, 100 cm long monochromatic UV lamp emitting at 253.7 nm. The treatment performances of the two photoreactors have been compared for a constant flow rate and constant UV lamp power. The lamp power is 484 W, which leads to 150 W of emitted UV power, by assuming 31% efficiency for the UV lamps. The UV lamps are surrounded by a 5.5 cm diameter quartz sleeve and the gap space between the lamp and quartz sleeve is occupied by air. While the modeled reactors are hypothetical, they can be considered the constitutive elements of large-scale, multi-lamp commercial photoreactors.

In both photoreactors, water composition whose characteristics are constant (25°C, phosphate esters 5 mg/L each, hydrogen peroxide 50 mg/L, bicarbonates 24 mg/L, buffered pH=7) were simulated by introducing the premixed solution at the reactor inlet at a volumetric flow rate of 2.1 m^3/h.

III. RESULTS AND DISCUSSION

A. Flow Distribution

Fig. 2 (a) and (b) display the velocity vectors for annular and cross-flow rectors, respectively. As expected, the velocity profile of the annular reactor (Figure 2a) is almost uniform resembling the well-known plug-flow reactor hydrodynamics. For the cross-flow reactor, however, the flow accelerates as it approaches the quartz sleeve (Fig. 2b) forming a large downstream recirculation region at around θ=90°. Also it is shown that the velocity in the cross flow

reactor is significantly smaller than the annular reactor, due to larger cross section in cross flow reactor. This leads to greater residence time of the particles in the cross flow reactor.

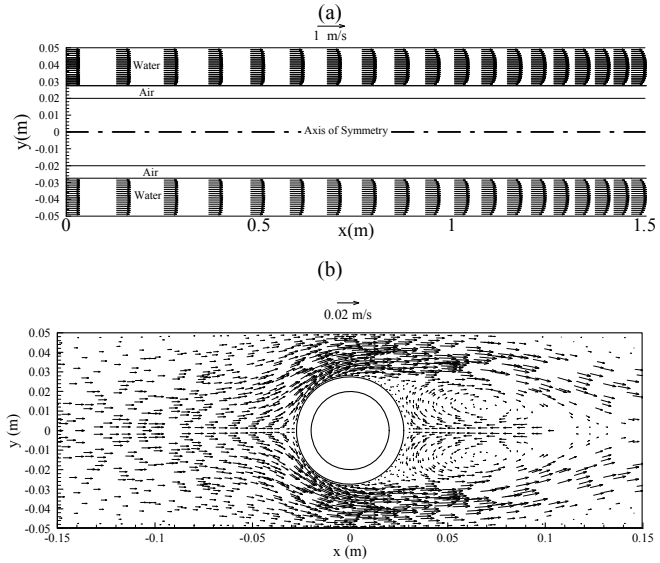

Fig. 2. Velocity vectors for: a) annular UV reactor and b) cross-flow UV reactor

B. Fluence rate Distribution

The detailed fluence rate distributions for both reactors employing a 484 Watt UVC lamp a volumetric flow rate of Q=2.1 m^3/h, and a 50 mg/L H_2O_2 concentration are presented in Figure 3. The fluence rate is solved using a fluid with spatially dependent water transmittance (UVT_{254}) which is a function of the H_2O_2 and HO_2^- molar concentration and their molar absorption coefficients.

Notably, the fluence rate is still dominated by the emission characteristic of the UV source considering the relatively small changes of the fluid absorption coefficient undergoing hydrogen peroxide photolysis.

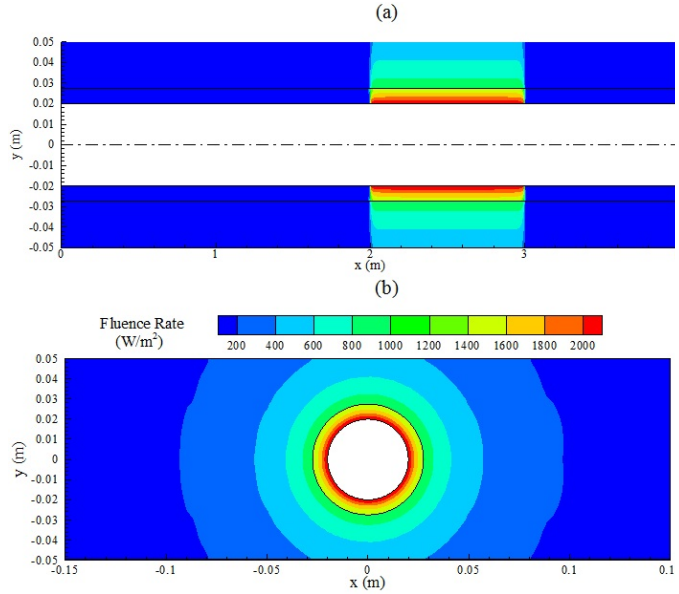

Fig. 3. Fluence rate contours for: a) annular UV reactor and b) cross-flow UV reactor

For both reactors, the fluence rate contours in proximity of the quartz sleeve (y=0.0275 m, r=0.0275 m) reveals a slight discontinuity at the air-water interface due to refraction.

C. H_2O_2 Distribution

The predicted contours of hydrogen peroxide for the annular reactor are presented in Fig.5 (a). Only minor changes in H2O2 concentration occur in the first part of the photoreactors (i.e. x<2 m) where the fluence rate is very low (Fig. 3, a) while a considerable spatial variation in H2O2 photolysis takes place in the central portion of the system (2 m<x<3 m).

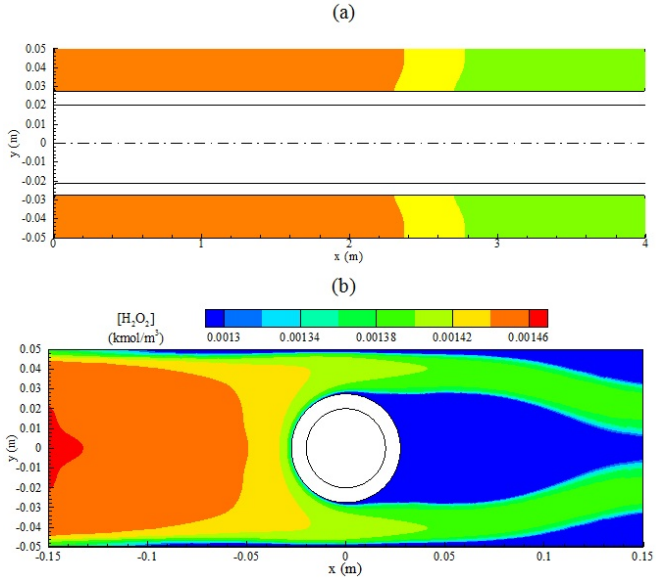

Fig. 4. Molar concentration of H_2O_2 for: a) annular UV reactor and b) cross-flow UV reactor

Cross-flow photoreactor results, illustrated in Fig. 5 (b), showed that hydrogen peroxide concentration starts to decrease as fluid approaches the irradiated zone around the cylindrical quartz sleeve. In this reactor configuration, significant gradients of peroxide concentration are observed in the radial direction.

D. OH• Distribution

Contours of hydroxyl radical concentrations are presented in Fig. 5. In both cases, the regions of high hydroxyl radical concentration resulted from both the complex generation and termination reactions and from the transport phenomena occurring in the UV-H2O2 photoreactors with significant concentration gradients displayed in the radial direction.

The corresponding results for the cross-flow reactor, shown in Fig. 6 (b), confirmed higher hydroxyl radical levels in proximity of the sleeve (see Fig.4. b). Contours of hydroxyl radicals are elongated in the direction of the flow due convective transport occurring in the system.

E. TCEP and TBP Distribution

Contaminant contours are presented in Fig. 6 (TCEP) and Fig. 8 (TBP). In both cases, the steady state contaminant and hydrogen peroxide distributions showed considerable similarity (Fig. 4 and 6). Moreover, the yield of TBP removal was found to be considerably higher than that of TCEP due to its higher hydroxyl radical rate constants (i.e., $k_{TBP} = 6.4\times10^9 M^{-1}s^{-1}$, $k_{TCEP} = 5.6\times10^8 M^{-1}s^{-1}$).

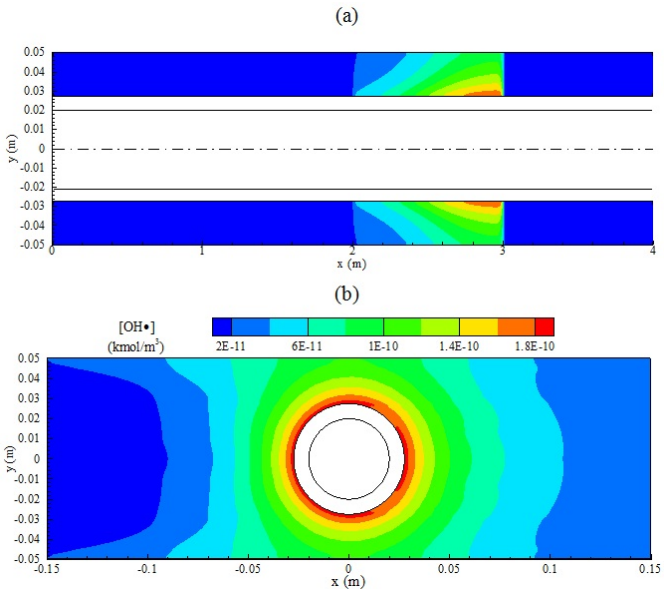

Fig. 5. Molar concentration of [OH•] through the (a) annular and (b) cross-flow reactors

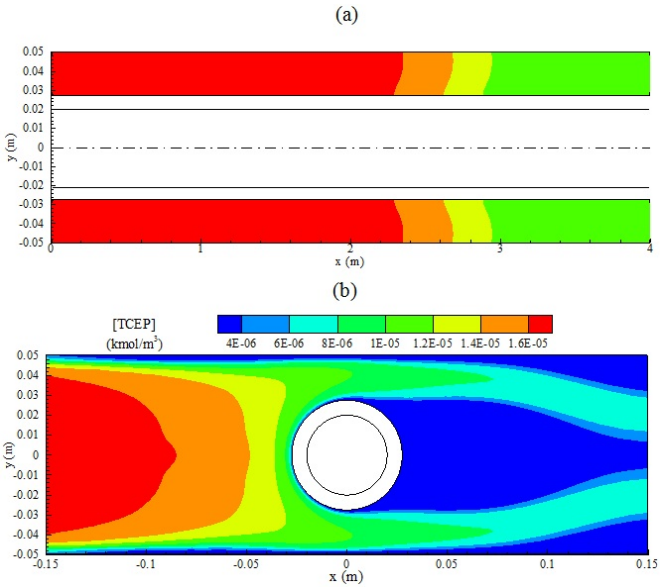

Fig. 6. Molar concentration of TCEP for: a) annular UV reactor and b) cross-flow UV reactor

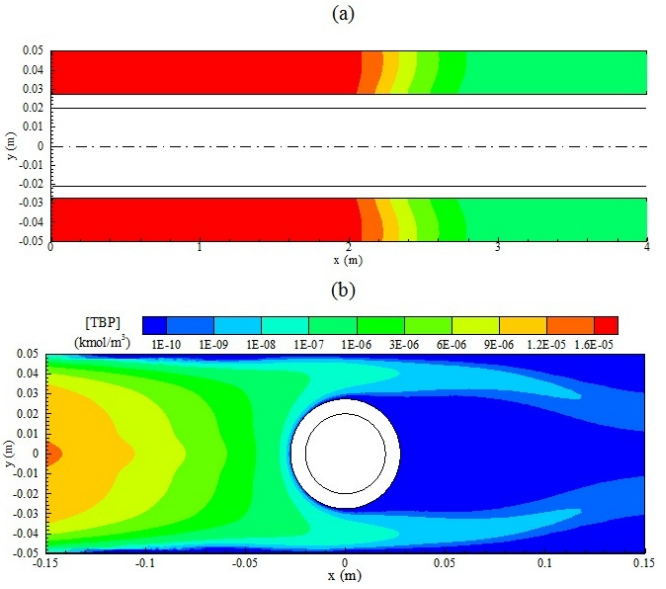

Fig. 7. Molar concentration of TBP for: a) annular UV reactor and b) cross-flow UV reactor.

Comparing the contaminants removal in annular and cross flow reactors, shows that in identical physical conditions the cross flow reactor is more efficient than the annular reactor.

F. Energy Consumption

To investigate the efficiency of the reactors, the Electrical Energy per contaminant degradation Order (EEO) is computed for different contaminant rates. Fig. 9 shows the EEO for annular and cross flow reactors with different contaminant rates. As it is expected, it is shown that the EEO reduces significantly by increasing the contaminant rate constant. Moreover it is found that the EEO of annular reactor is about 3 times greater than the cross flow reactor. This is due to the fact that the cross flow reactor have larger cross section (the volume of the cross flow reactor is greater than the annular reactor) and thus the velocity of the water in the cross flow reactor is smaller than the annular flow reactor. So the residence time of the particles in cross flow reactor is greater and the contaminants are disinfected more efficiently. Also it is found that unlike TCEP ($k_{TCEP} = 5.6\times10^{8}\, M^{-1}s^{-1}$) which at 50 mg/L initial hydrogen peroxide concentration requires an EEO ranging from 0.511 (cross-flow reactor) kWh/m^3 to 1.407 (parallel-flow reactor) log TCEP^{-1}, the oxidation of TBP ($k_{TBP} = 6.4\times10^{9}\, M^{-1}s^{-1}$) was achieved in a cost-effective manner using an order of magnitude lower energy consumption (EEO = 0.113 and 0.063 kWh/m^3 log TBP^{-1}).

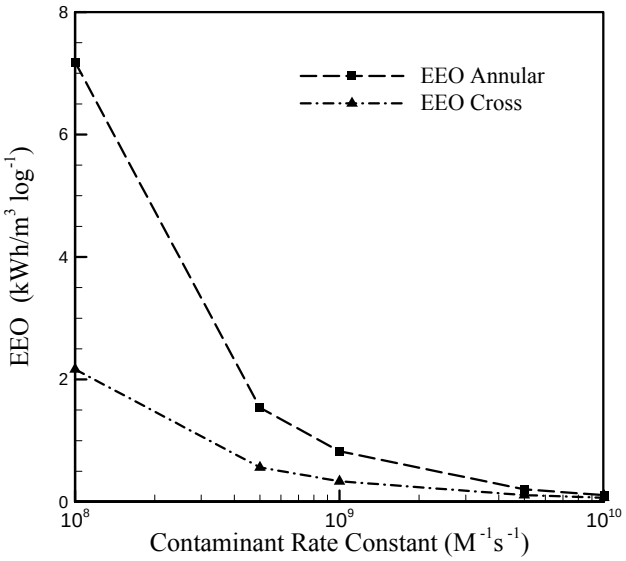

Fig. 8. Impact of hydroxyl radical rate constant on EEO

IV. Conclusions

In this paper, annular and cross flow UV-H_2O_2 photo reactors are numerically investigated using a comprehensive CFD models. Hydrodynamic, radiation and chemical reactions are modeled precisely and the effects of these models are considered on each other. It is found that the numerical results are consistent experimental data. Moreover the CFD model reveals the recirculation zone in cross flow reactor and shows the spatial contours of the chemical components and incident radiation. It is found that with identical conditions the cross flow reactor has better disinfection performance. Also the electrical energy

consumption of the photo reactors is investigated and it is found that the cross flow reactor is more efficient than the annular reactor. This is due to the greater residence time of the particles in the cross flow reactor and it can be concluded that using larger photo reactors can reduce the EEO significantly.

REFERENCES

[1] Stefan, M. I., A. R. Hoy, and J.R. Bolton, "Kinetics and Mechanism of the Degradation and Mineralization of Acetone in Dilute Aqueous Solution Sensitized by the UV Photolysis of Hydrogen Peroxide". *Environmental Science & Technology*, 1996. 30(7): p. 2382-2390.

[2] Crittenden, J. C., S. Hu, D. W. Hand, and S.A. Green, "A kinetic model for H_2O_2/UV process in a completely mixed batch reactor". *Water Research*, 1999. 33: p. 2315-2328.

[3] Watts, M. J. and K. G. Linden, "Photooxidation and subsequent biodegradability of recalcitrant tri-alkyl phosphates TCEP and TBP in water". *Water Research*, 2008. 42(20): p. 4949-4954.

[4] Bolton, J. R., "Calculation of ultraviolet fluence rate distributions in an annular reactor: significance of refraction and reflection". *Water Research*, 2000. 34(13): p. 3315-3324.

[5] Liu, D., J. Ducoste, S. Jin, and K. Linden, "Evaluation of Alternative Fluence Rate Distribution Models". *Journal Water Supply and Research-AQUA*, 2004. 53(6): p. 391-408.

[6] Sasges, M., R., A. van der Pol, A. Voronov, and J. Robinson, "*A Standard Method for Quantifying the Output of UV Lamps"*, in *International Ozone Association Joint Congress*2007, International UV Association.

[7] Sozzi, D.A. and F. Taghipour, "Computational and experimental study of annular photo-reactor hydrodynamics". *International Journal of Heat and fluid flow*, 2006. 27(6): p. 1043-1053.

[8] Shao, L., "*Degradation of 4TBP by AOP, UV Reactor Modeling and Validation, Master Thesis"*, in *Faculty of Civil Engineering and Geosciences, Section Water Management*2007, Delft University of Technology.

[9] Hofman, J., et al., "*Design of UV reactors by CFD: Model Development and Experimental Validation"*, in *Proceedings of the COMSOL Users Conference, Grenoble*2007.

[10] Alpert, S., D. Knappe, and J. J. Ducoste, "Modeling of UV/Hydrogen Peroxide Advanced Oxidation Processes using Computational Fluid Dynamics". *Water Research*, 2010. 44(6): p. 1797-1808.

[11] Reemtsma, T., et al., "Polar Pollutants Entry into the Water Cycle by Municipal Wastewater: A European Perspective". *Environmental Science & Technology*, 2006. 40(17): p. 5451-5458.

[12] Kolpin, D.W., et al., "Pharmaceuticals, Hormones, and Other Organic Wastewater Contaminants in U.S. Streams, 1999-2000: A National Reconnaissance". *Environmental Science & Technology*, 2002. 36(6): p. 1202-1211.

[13] Li, K., J. C. Crittenden, D.W. Hand, and D. R. Hokanson, "*Advanced Oxidation Process Simulation Software (AdOx) Manual, Version 1.0"*, 2002: Michigan Technological University.

[14] Modest, M. F., *Radiative Heat Transfer*1993: Series in Mechanical Engineering. McGraw-Hill.

[15] Baxendale, J. H. and J. A. Wilson, "The photolysis of hydrogen peroxide at high light intensities". *Transactions of the Faraday Society*, 1957. 53: p. 344-356.

[16] Buxton, G. V., C. L. Greenstock, W. P. Helman, and A. B. Ross, "Critical review of rate constants for reactions of hydrated electrons, hydrogen atoms and hydroxyl radicals in aqueous solution". *Journal of Physical and Chemical Reference Data*, 1988. 17(2): p. 513-886.

[17] Christensen, H. S., H. Sehensted, and H. Corfitzan, "Reactions of hydroxyl radicals with hydrogen peroxide at ambient and elevated temperatures". *Journal of Physical Chemistry*, 1982. 86: p. 55-68.

[18] Koppenol, W. H., J. Butler, and J.W. Van Leeuwen, "The Haber-Weiss cycle". *Photochemistry and Photobiology*, 1978. 28(4-5): p. 655-660.

[19] Weinstein, J. and B. H. J. Bielski, "Kinetics of the interaction of HO_2 and O_2^- radicals with hydrogen peroxide. The Haber-Weiss reaction". *Journal of the American Chemical Society*, 1979. 101(1): p. 58-62.

[20] Draganic, Z. D., et al., "Radiolysis of aqueous solutions of ammonium bicarbonate over a large dose range". *Radiation Physics and Chemistry*, 1991. 383: p. 21-317.

[21] Sehested, K., O. L. Rasmussen, and H. Fricke, "Rate constants of OH with HO_2, O_2^- and $H_2O_2^+$ from hydrogen peroxide formation in pulse-irradiated oxygenated water". *Journal of Physical Chemistry*, 1968. 72(2): p. 626-631.

[22] Bielski, B. H. J., D. E. Cabelli, R. L. Arudi, and A. B. Ross, "Reactivity of HO_2/O_2^- radicals in aqueous solution". *Journal of Physical and Chemical Reference Data*, 1985. 14(4): p. 1041-1100.

[23] Beck, G., "Elektrishe leitfaehigkeits messungen zum nachweis geladener zwischenprodukte der pulsaradiolyse". *Int. J. Radiat. Phys. Chem.*, 1969. 1(3): p. 361-371.

[24] Holeman, J., E. Bjergbakke, and K. Sehested, "The importance of radical-radical reactions in pulse radiolysis of aqueous carbonate/bicarbonate". *Proc. Tihany Symp. Radiat. Chem.*, 1987. 61: p. 53-149.

[25] Eriksen, T. E., J. Lind, and G. Merenyi, "On the acid-base equilibrium of the carbonate radical". *Radiation Physics and Chemistry*, 1985. 26(2): p. 197-199.

[26] Huie, R. E. and C. L. Clifton, "Temperature dependence of the rate constants for reactions of the sulfate radical, SO_4^-, with anions". *Journal of Physical Chemistry*, 1990. 94(23): p. 8561-8567.

[27] Watts, M. J. and K. G. Linden, "Advanced Oxidation Kinetics of Aqueous Trialkyl Phosphate Flame Retardants and Plasticizers". *Environmental Science & Technology*, 2009. 43(8): p. 2937-2942.

[28] Stumm, W. and J. J. Morgan, *Aquatic Chemistry*1996, Engelwood, NJ: Prentice-Hall.

[29] Perry, R. H., D. W. Green, and J. D. Maloney, *Perry's Chemical Engineers' Handbook*. 5 ed1981, New York: McGraw-Hill.